

Comparison of PV Inverter Controller Configurations for CERTS Microgrid Applications

Micah J. Erickson
Student Member
mjerickson@wisc.edu

T. M. Jahns
Fellow
jahns@engr.wisc.edu

Robert H. Lasseter
Fellow
lasseter@engr.wisc.edu

Dept. of Electrical and Computer Engineering
University of Wisconsin – Madison
Madison, WI 53706 USA

Abstract – Microgrids are highly compatible with photovoltaic (PV) sources because of their ability to internally aggregate and balance multiple PV sources without imposing restrictions on the penetration of such intermittent power sources. There are two major types of inverter control configurations that are used in photovoltaic inverters to provide an interface to a CERTS microgrid. These control configurations exhibit important duality characteristics, and both are capable of tracking maximum input power while abiding by the CERTS droop algorithms. This paper investigates and demonstrates the comparative performance characteristics of these two major controller types: 1) a grid-forming droop-style controller similar to those used for controlling distributed generators; and 2) a current-regulated grid-follower controller. It is shown that only the grid-forming controller allows a PV source to operate alone in an islanded CERTS microgrid, but the grid-follower controller enjoys some inherent advantages with regard to faster dynamic response.

Index Terms—Photovoltaic, PV, CERTS, energy storage, inverter, microgrid, grid forming, grid following.

NOMENCLATURE

uSrc	Microsource droop-controlled source
CERTS	Consortium for Electric Reliability Technology Solutions

I. INTRODUCTION

Microgrids have basic features that make them attractive candidates for aggregating various types of renewable energy (RE) and conventional power sources, even if the RE sources are intermittent [1]. The CERTS microgrid concept [2] utilizes power-versus-frequency droop and reactive power-versus-voltage droop to provide a stable electric grid during islanded operation without additional inter-source communications. Stable power operating points are achieved in this type of microgrid by introducing grid-forming (droop-style) sources that are designed to implement power vs. frequency droop characteristics. This droop adjusts the relative load angle across a coupling inductance between two voltage sources in order to control the power flow. In

addition, reactive power vs. voltage droop is implemented to control the reactive energy delivered by the microgrid sources while regulating the microgrid voltages to acceptable levels.

While a variety of source types have been evaluated for use in a microgrid, photovoltaic (PV) inverters present some unique source characteristics. A microgrid is invariably rich in transients and needs to be reconfigurable to readily support the growth and intermittency of distributed generation installations. As a result, the microgrid creates a changing power system environment to which the PV inverter must continuously adapt while exhibiting stable response characteristics. Introduction of a PV source into a microgrid makes it necessary to accommodate both the wide power variability of solar radiation as well as the frequency and system load variations that are typical in a microgrid environment. Previously published work in this area has addressed either the PV source variability or the microgrid voltage and frequency adjustments as separate issues, but not together [3].

Conventional grid-tied PV inverters are typically designed to always operate at unity power factor by injecting a prescribed current in phase with a 3-phase voltage vector. In contrast, the inverters used in CERTS microgrids typically employ a voltage-source based droop-style controller topology that varies its frequency in direct proportion to the output power and voltage magnitude in response to reactive power changes. The controllers associated with these two types of inverters represent two contrasting approaches to creating a microgrid-compatible PV inverter because they reverse the roles of current and frequency between measured values and controlled output quantities.

The purpose of this paper is to evaluate and compare the key performance characteristics of these two controller types in a CERTS microgrid environment. It will be shown that the droop-style controller exhibits a lower power control bandwidth due to the basic limitations of angle-only control that are inherent in the droop-style controller configuration. In contrast, the current-regulating (also referred to as grid-

following) controller is incapable of operating alone in an islanded configuration without another grid-forming source in the same microgrid to stabilize the voltage amplitude and frequency. Multiple analytical tools including dynamic simulation are combined with experimental verification to evaluate the alternative controllers and confirm their operating characteristics.

II. CHALLENGES POSED BY PV SOURCES IN MICROGRIDS

An example of a PV source combining PV cells with a voltage-source inverter, output filter, and isolation transformer is presented in Fig. 1. This configuration has been selected as the baseline for this investigation since it is both simple as well as commonly applied in commercially-available PV inverters.

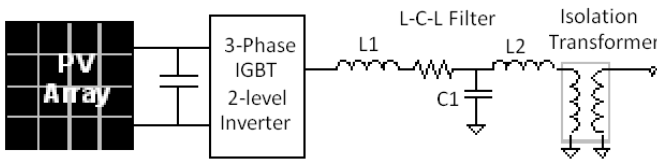


Figure 1 – Baseline PV source configuration showing 3-phase voltage-source inverter and 1-line filter diagram with isolation transformer

Photovoltaic cells vary their voltage output with irradiance, temperature, and current loading (Fig. 2) [10]. There is a clearly defined maximum power per cell and very little dynamic delay associated with the PV cell itself. While the maximum power point voltage is shown here to vary only slightly with irradiance, temperature has a significant effect that requires regulation of the DC voltage to achieve maximum power point tracking.

Economic incentives almost invariably make it imperative to operate the PV cells at their maximum power points whenever possible. This creates a special challenge since, unlike conventional synchronous generators, there is no stored energy available from the PV cells themselves to support the microgrid dynamic behavior during transient conditions. Therefore, any overload energy from the PV source, i.e., power drawn beyond the maximum power point of the array, must come from the very limited energy stored in the DC bus capacitance of the PV-inverter combination.

Typically, the DC bus capacitance energy in PV inverters is designed to be very small for economic reasons with values in the vicinity of 0.01 pu-seconds of energy. This figure implies that a DC bus voltage regulator would require fast response times in the range of 10 ms or less to maintain control and insure robust safe operating areas in response to 1 pu step load changes. The situation is proportionally less dire if the expected load variations are limited to less than 1 pu, but there is little basis for assuming here that the PV sources will be protected from large-scale power transients in real microgrid applications.

If the DC bus voltage falls from the maximum-power-point voltage to the minimum voltage required by the inverter

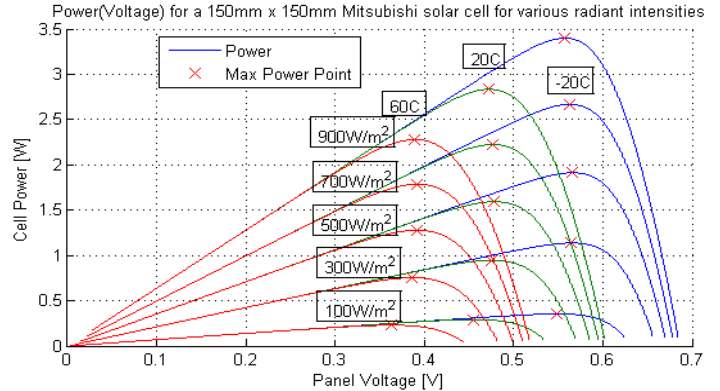


Figure 2 – Power vs. voltage characteristics of single PV cell under various insolation and temperature conditions, based on Mitsubishi solar cell. [10]

to deliver rated AC voltage at its output terminals, undesirable system effects occur that negatively affect microgrid operation. This limit-mode condition will cause uncontrolled reactive power to flow in the PV source and/or over-modulation of the PV inverter that leads to injection of undesirably high levels of line harmonics. Since the available stored energy is small in most cases, the power control bandwidth becomes a major design issue faced by both types of PV source controllers since they share the same basic voltage-source inverter topology.

The situation is further complicated by the fact that the PV power characteristic below the maximum-power-point voltage is unstable. That is, the power available from the PV cells decreases with any drop in the voltage below that of the maximum power point, increasing the difference in power between the AC and DC sides of the inverter and accelerating the voltage collapse.

From Fig. 2, it can be seen that there is a plateau region of small changes in power as a function of voltage near the maximum power point. As a result, the destabilizing effects caused by this power drop can be mitigated by maintaining the voltage as close to this region of near-constant maximum power as possible under all operating conditions. Unfortunately, this objective becomes even more difficult to achieve if a series array is partially shaded since such shading can cause the PV power to drop more steeply on both sides of the maximum power point as well as creating multiple local-maximum power points [6].

Summarizing, the controller must be designed to respond rapidly to large positive load transients by reducing the PV source output power below the PV cell array's maximum capability before the DC link voltage reaches its minimum design value in order to prevent uncontrolled currents and/or DC link voltage collapse from occurring. Preventing such uncontrolled shutdown events and maintaining stable and well-damped operation under all steady-state and dynamic load conditions are primary design objectives for both controller configurations.

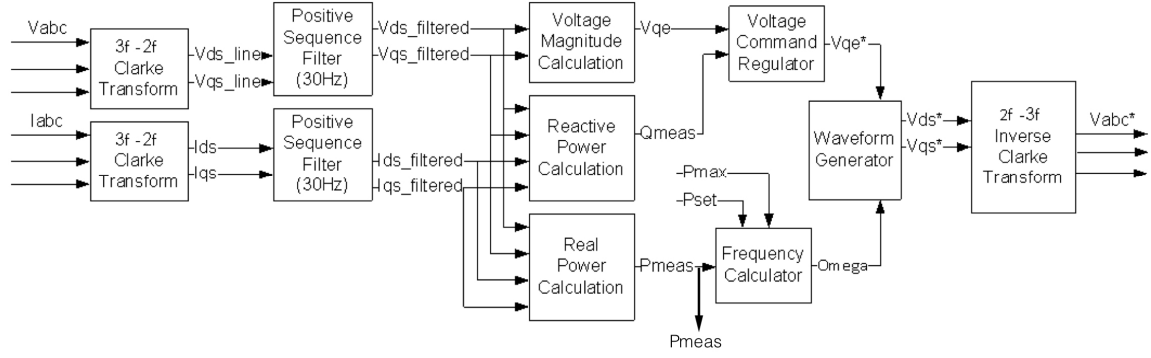


Figure 3 – Basic grid-forming droop-style inverter controller configuration (uSrc)

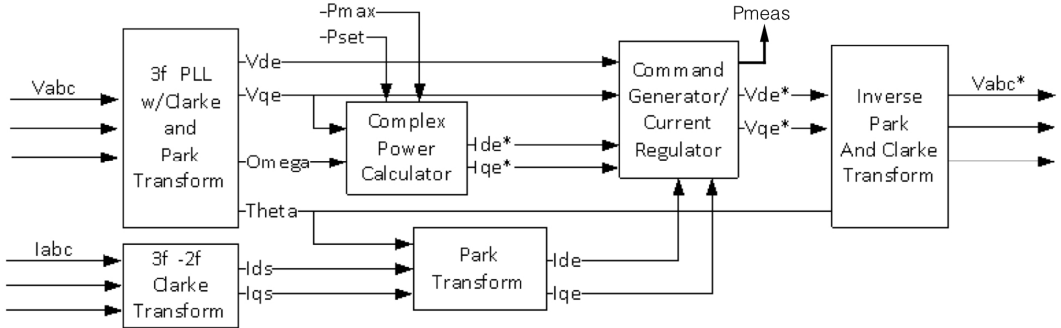


Figure 4 – Basic grid-following current-regulated inverter controller configuration

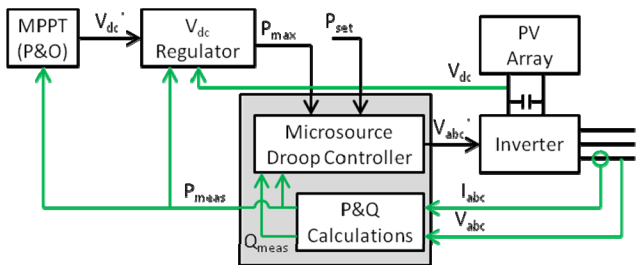


Figure 5 – PV microsource control diagram including voltage-based maximum power point tracking, DC bus voltage regulation, and the microsource droop controller that can be either grid-forming or grid-following.

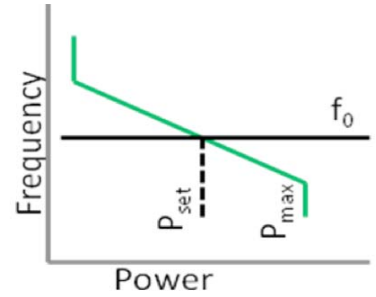


Figure 6 – Frequency vs power droop curve for grid-forming uSrc controller showing condition for which $P_{set} < P_{max}$

III. CONTROLLER CONFIGURATIONS

The overall control configuration for the PV sources in CERTS microgrids is provided in Fig. 5. The controls consist of three key segments. The maximum power point tracking (MPPT) controller in the upper left of the figure is responsible for developing the setpoint for the inverter DC link voltage V_{dc}^* (which is also the PV array output voltage) in order to extract maximum delivered power from the PV array whenever possible. The DC link voltage regulator to the right of the MPPT controller in Fig. 5 is responsible for regulating V_{dc} to its setpoint value V_{dc}^* by adjusting the maximum power limit P_{max} . This P_{max} value determines the average inverter output power whenever the load is capable of absorbing the maximum PV array power.

The innermost control loop is the microsource controller shown in the central grayed block in Fig. 5. While both PV source topologies are identical as shown in Fig. 1 and the right side of Fig. 5, the two types of microsource controllers investigated in this work exhibit important quality characteristics.

The droop-style controller (referred to henceforth as a uSrc controller) shown in Fig. 3 represents the traditional implementation of microsources in a CERTS microgrid [1]. It operates similarly to a synchronous generator with the exception of physical inertia. The frequency and magnitude of the three-phase output voltage vector is varied based on the measured real power and reactive power delivered by the source, respectively. Each changes according to a programmed value of droop as in [2].

The frequency vs. power droop relationship for the grid-forming uSrc controller is shown in Fig. 6. The vertical bias position of the curve is shifted without changing the slope so that the nominal frequency of the microgrid f_o (typ. = 60 Hz) falls on the droop curve at P_{set} . As the value of P_{max} delivered by the output of the voltage regulator changes, the right-side vertical power limit line shifts left and right. The instantaneous value of P_{meas} determines where on the droop curve that the PV microsource operates at any time instant.

The “Voltage Command Regulator” block in Fig. 3 includes a closed-loop voltage regulator that first forms the error between the measured AC voltage amplitude V_{qe} and the voltage amplitude command delivered by the voltage-vs-reactive power droop function. This error is then passed through a PI regulator block in order to develop the voltage amplitude command V_{qe}^* required by the inverter. The values of these gains influence the reactive power control bandwidth of the grid-forming controller.

The alternative current-regulating controller shown in Fig. 4 reverses the roles of the control variables so that the output current, serving as the surrogate for the output power, is the controlled variable. The current amplitude and waveshape is determined by the measured voltage magnitude and observed frequency to maintain compatibility with CERTS microgrid droop concepts. That is, the two axes of the droop characteristic in Fig. 6 are reversed so that the observed frequency of the terminal voltages provides the input to determine the commanded inverter output power using the inverted droop curve. The current amplitude command corresponds to this power divided by the network voltage.

It should be noted that the grid-following controller in Fig. 4 has a reactive power droop characteristic like the grid-forming controller. The d-axis output current (90 degrees lagging the voltage) of the grid-following PV microsource is controlled to be proportional to the difference between the measured voltage and the rated system voltage.

Each controller has the same MPPT algorithm and implementation that behaves as a slower outer control loop wrapped around the frequency-vs-power relationships that are programmed into each of the inner-loop microsource controllers. The base MPPT algorithm is a ‘perturb and observe’ (P&O) algorithm that commands small changes in the DC bus voltage (perturb), pauses for voltage convergence, then measures the power (observe) to determine if the perturbation direction correctly resulted in higher output power [12]. For the transient time scale that is investigated in this work, the details of the MPPT algorithm will not be discussed further here since it is covered in depth in the technical literature.

However, the method by which the DC bus is regulated is of importance to this discussion. Whenever the PV array is

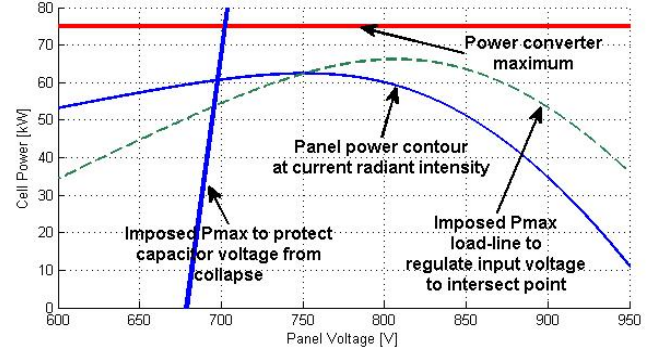


Figure 7 – Calculated plots of the PV array output power-vs-voltage and P_{max} -vs-voltage curves for a DC bus voltage command of 750Vdc, illustrating the regulation mechanism that drives the voltage error to zero.

asked to deliver its maximum power, the instantaneous AC inverter output power is adjusted with respect to the PV array power in order to regulate the bus voltage V_{dc} to its commanded value from the MPPT algorithm. The voltage regulator equation is

$$P_{max}(k) = P_{meas}(k) - K_{pv} [V_{dc}(k)^* - V_{dc}(k)] - K_{dv} [V_{dc}(k-1) - V_{dc}(k)] \quad (1)$$

where P_{max} is the output of the voltage regulator that sets the maximum power limit of the power-vs-frequency droop curve in Fig. 6, P_{meas} is the measured inverter three-phase output power that serves as an offset for developing the P_{max} output value, K_{pv} is the voltage regulator proportional gain value that converts the DC bus voltage error to output power command, and K_{dv} is the gain of a derivative controller term that provides the damping of the voltage regulator response.

The steady-state relationship between P_{max} and the DC bus voltage is determined by adding the amplified bus voltage error term from (1) to the power-vs-voltage characteristic of the PV array (Fig. 2). Figure 7 shows both of these curves for a sample case with a commanded DC bus voltage V_{dc}^* of 750Vdc, the equilibrium voltage value at which the two curves intersect. For V_{dc} values larger than this command value, the maximum inverter output power will exceed the PV array power delivered to the bus, causing the bus voltage to decrease so that the error is driven towards zero. The inverse situation exists when V_{dc} is less than V_{dc}^* , causing the bus voltage to increase towards the command value. The value of the proportional gain K_{pv} determines the rate of divergence of the two power curves as the voltage error amplitude increases, indicating how rapidly the voltage error is driven towards zero.

This scenario ideally results in well-behaved linear control of the DC bus capacitor current proportional to the error between the commanded V_{dc}^* and measured V_{dc} . Assuming that the power regulator bandwidth is sufficiently high, the DC bus voltage response is first-order. However, in cases where the power regulation bandwidth is within an order of

magnitude of the bandwidth of the DC bus voltage regulator, second-order capacitor voltage responses are developed. The derivative controller term that appears in (1) helps to improve the voltage dynamic response under these conditions.

IV. CONTROLLER IMPLEMENTATION RESULTS

Among the various transients that can be applied to evaluate the controller response characteristics, a particularly informative transient is the step load increase in an islanded system. In contrast, grid-connected system transient results are limited in the information they can provide since the ‘infinite grid’ absorbs the majority of the initial load transient. Furthermore, the grid frequency does not vary in response to the load transient, preventing such transients from testing the ability of the converter to respond to network frequency changes.

In addition, suddenly increasing the load tests the performance impact of the destabilizing PV power-vs-voltage characteristic in the vicinity of its maximum power point. In contrast, sudden decreases in load naturally result in an upward surge in the DC bus voltage that automatically reduces the input power from the PV array, serving as a passive mechanism that helps to re-establish a new steady-state operating point. Therefore, a positive load transient in an islanded system is more effective for exploring the response under worst-case operating conditions.

The simple islanded microgrid that is studied here consists of an Energy Storage (ES) microsource with a standard droop-based controller together with a PV microsource, composing a two-source 480Vrms network. Each microsource consists of a 3-phase inverter that is supplied by a DC energy/power source. Each source has a 15kVA power rating and values of the key PV inverter components in Fig. 1 are provided in the Appendix, together with controller gains.

The photovoltaic array has a maximum power rating of 15kW. It consists of 138 individual panels that house the polycrystalline Mitsubishi solar cells modeled in Fig. 2 [10]. The ES source is supplied by a 7.5kW, 7.5kWh battery. Its power restrictions are neglected in this simulation in order to focus on the displayed dynamics of the PV source. This means that the ES source will always operate along the linear droop portion of its frequency vs. power droop characteristic.

Finally, a resistive load is connected at the midpoint of the cable connection between the PV array and the battery ES microsources.

Simulation of Step Load Increase Response

Figure 8 shows Electromagnetic Transients Program (EMTP) simulation results for a positive load transient from 12kW to 18.5 kW applied to the islanded microgrid with both types of controllers for the PV microsource. The base power for the adopted per-unit system is 15kW and the base voltage for the DC link voltage is 750 Vdc. Traces are overlaid for the responses with the two types of PV

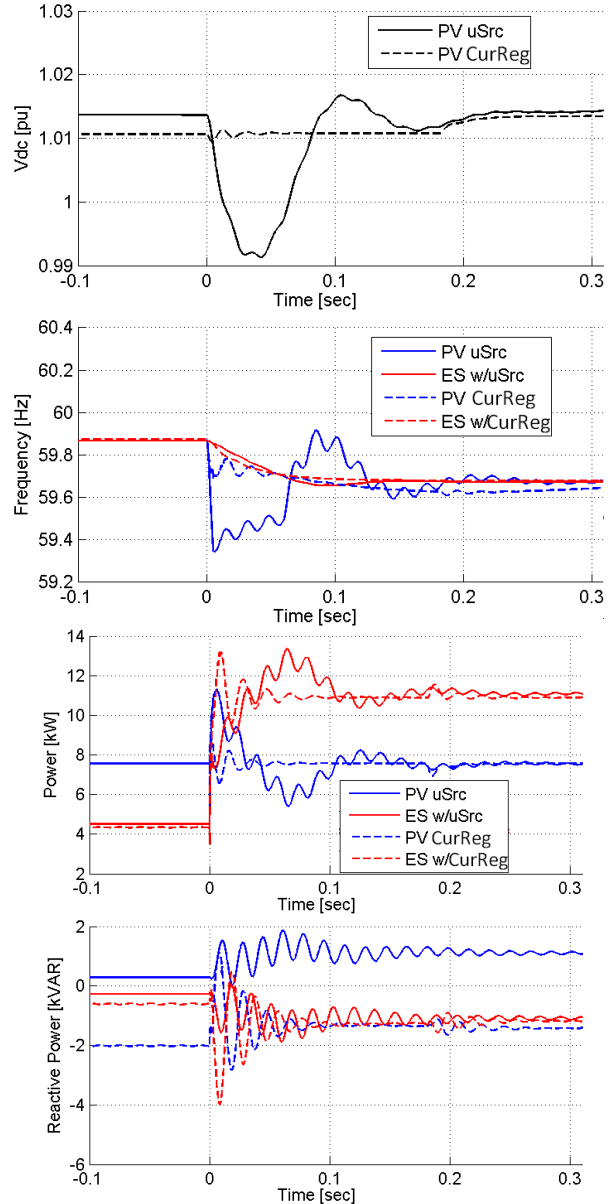


Figure 8 – Simulated power, reactive power, DC bus voltage, and frequency dynamic response comparisons for the two PV controller cases for a 6.5 kW (0.43pu) positive load transient in an islanded microgrid.

controllers to simplify the comparisons. The primary observation drawn from this comparison is the considerably slower power control bandwidth of the uSrc controller that is limited by the droop controller gain. This gain limit is imposed to avoid exciting oscillatory network responses that can occur due to droop-style control schemes [3].

The transient changes in all four variables in Fig. 8 are significantly larger for the uSrc with the droop-style controller due to its lower power control bandwidth compared to the grid-following controller case. The frequency and the power responses exhibit 60Hz oscillations that are caused by the unbalanced excitation of the line inductors after a frequency change, resulting in a significant transient phase

offset. The decay rate of the 60Hz component is proportional to the resistance-to-reactance ratio of the line connecting the two sources that are experiencing this power oscillation.

Although not shown in Fig. 8, the energy storage source, operating within the limits of its power range, exhibits fast, well-behaved damping in its frequency response. This desirable behavior can be attributed to its constant linear power-vs-frequency droop gain, set at 0.5 [Hz/pu Power].

Experimental Results for Step Load Increase

Figure 9 shows measured test results for the same positive load transient applied to an experimental microgrid system, providing a comparison of the response with the two types of PV controllers. The emulated PV source is the key component under test. It is fed by a DC power supply with a controllable current limit that emulates the V-I profile of a uniformly insulated PV array.

To accompany the PV emulator source, an energy storage source is configured as a bi-directionally adjustable microsource. It is initially set to a mode where it is slightly charging prior to the load application and then discharging at the new steady-state operating point after the load is applied to allow the PV source to maintain constant maximum power output for this test.

In practice, the energy storage source will eventually hit a limit if the applied load transients are sufficiently large. A positive limit with a load that exceeds the combined power capability of the PV and ES microsources would cause a voltage collapse if the load cannot be shed in time. In contrast, hitting the negative power limit leads to a stable operating point for which the PV source automatically moves away from its MPPT operating point and reduces its power output as much as necessary.

Test results from applying a positive load transient from zero to 5.6kW to the experimental microgrid are provided in Fig. 9. The recorded DC bus regulation waveforms exhibit features that are similar to those in Fig. 8 where the current-regulated converter more tightly regulates the DC bus than the droop-style controller. While the microsource (uSrc) shows a slightly less damped and larger DC voltage excursion than the simulation, the response of the current-regulated source matches the simulated response quite closely. The maximum dc bus voltage excursion is approx. 0.5% and the transient lasts less than two cycles.

Conversely, the significantly lower power control bandwidth and smaller damping factor of the uSrc controller is evident in the waveforms and similar to simulation. The lower damping factor in the measured uSrc response compared to the simulation can be attributed in part to the impact of the current regulator dynamics of the power supply used in the PV emulator. In addition, noise in the DC bus

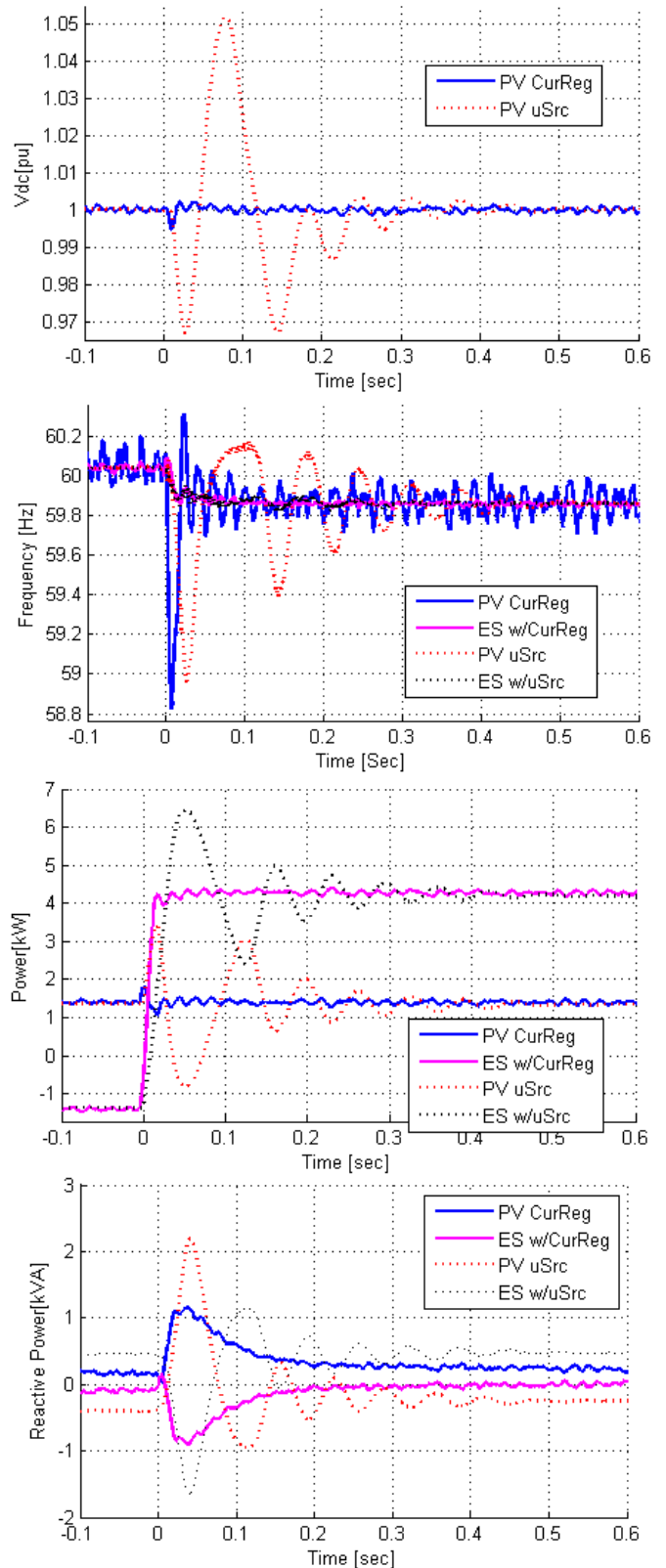


Figure 9 – Measured power, reactive power, DC voltage and frequency dynamic response comparisons for hardware implementation of an islanded microgrid following application of a positive 5.6kW (0.37pu) load step.

voltage sensor signal limited the gain K_d that could be used in the derivative portion of the voltage regulator in Eqn. (1) without causing forced oscillations in the response.

The measured frequency waveforms in Figure 9 show the rapid response of the current-regulated microsource in comparison to the droop-based uSrc case, although they both settle to the same new operating frequency within approx. 0.3s. The uSrc frequency exhibits a flat plateau beginning at approx. 100ms after the load is applied caused by a brief period of controller operation in its linear droop region after the power limit control integrator in the frequency calculator [1] of Fig. 3 has unwound and disengaged briefly. The slower-acting energy storage source has a much more well-behaved frequency characteristic in response to the transient which is expected considering its much higher amount of stored energy compared to that of the DC bus capacitors in the PV inverter.

The measured power traces in Fig. 9 illustrate the superior dynamic stiffness of the current-regulated photovoltaic source in the face of load transients, although the transient power response of the uSrc controller is relatively well-damped. The measured reactive power waveforms exhibit a similar trend, settling to the new steady-state operating point sooner with the current-regulated source. In fact, the transient response of the current-regulated reactive power is primarily determined by the DC bus voltage regulator. In contrast, the droop-based uSrc microsource exhibits significant oscillations in both the reactive and active power responses that, in part, are caused by the network resistance causing cross-coupling between reactive power and load angle.

Experimental Results for Step Load Decrease

Figure 10 shows the measured waveforms for the complementary case of a step load decrease. That is, the 5.6kW load (corresponding to 0.37pu) is removed, causing a transient surge in the DC bus voltage of the PV inverter. Similar to the previous case of a positive load transient, it can be seen that the DC bus voltage is much less tightly regulated in the uSrc case, exhibiting a brief 4% surge immediately following the load decrease (with 0.15pu distributed initially to each source on a transient basis).

The measured frequency waveform in Fig. 10 exhibits a brief positive frequency spike for the current-regulated controller in order to keep it in phase with the voltage of the load following the load step. Some of the high-frequency oscillation in the frequency waveforms, particularly for the current-regulated controller case, can be attributed to $L-C$ filter oscillations and phase unbalance during post-processing of the measured AC voltage data. The frequency waveform for the droop-based uSrc controller again exhibits plateau behavior when it ventures into the linear droop region from $t=25\text{ms}$ to 125ms .

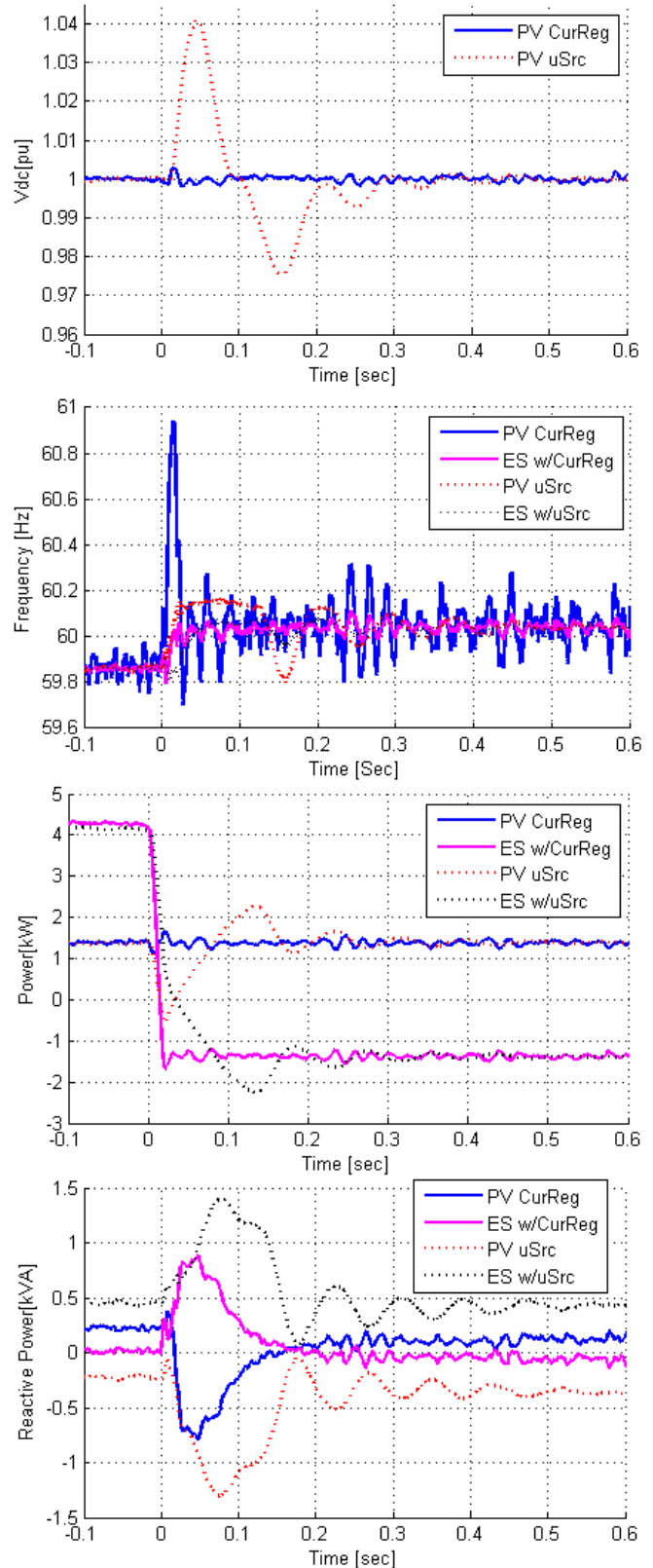


Figure 10 – Measured power, reactive power, DC voltage and frequency dynamic response comparisons for hardware implementation of an islanded microgrid following application of a negative 5.6kW (0.37pu) load step.

The power characteristics are largely consistent with those presented previously for the load step increase case. It should be noted that the load decrease transient illustrates the source shedding abilities of the PV source to avoid over-powering the network. The well-behaved response for both types of controller in Fig. 10 confirm that the PV control scheme transitions smoothly out of MPPT operation when necessary, and this transition does not play a significant role in overall power response behavior. This bodes well for potential microgrid operation of PV sources with either type of controller in a transient-rich environment.

Overall, both types of PV controllers behaved stably in response to both positive and negative load transients. The current-regulated controller has demonstrated its superior dynamic response characteristics for DC bus voltage and power regulation while still maintaining the ability to source-shed when necessary. However, the demonstrated ability of the grid-forming uSrc controller to execute its droop algorithms is critical to confirming the readiness of PV microsources to actively participate in maintaining stable CERTS microgrids when necessary.

V. CONCLUSION

This investigation has examined the performance characteristics of two major types of controller configurations for PV sources that are both appropriate for use in CERTS microgrids. Each controller configuration has demonstrated its ability to respond stably in the microgrid environment. While the uSrc controller suffers from larger DC bus voltage excursion issues during load transients due to its inherent power control bandwidth limitations, the current-regulating controller lacks the basic ability to operate alone in an islanded CERTS microgrid due to its inability to independently establish a reference operating frequency.

Both controllers have demonstrated their abilities to withstand the transient conditions associated with microgrid operation without significant additions of bus capacitance beyond what is typical for an industrial inverter. Therefore, the controller configuration selection depends on the microgrid design objectives for specific applications, requiring consideration of the engineering tradeoffs between fast dynamic response characteristics and high microgrid reliability/robustness.

REFERENCES

[1] Lasseter, R.H.; Paigi, P., "Microgrid: a conceptual solution," in *Proc. of 2004 IEEE Power Electronics Specialists Conference (PESC)*, vol.6, no., pp. 4285-4290, 20-25 June 2004.
 [2] Lasseter, R.H., "Extended CERTS microgrid," in *Proc. of 2008 IEEE Power and Energy Society General Meeting - Conversion and Delivery of Electrical Energy in the 21st Century*, 20-24 July 2008.

[3] Hui Zhang, et al, "Three-phase grid-connected photovoltaic system with SVPWM current controller," in *Proc. of Power Electronics and Motion Control Conference*, May 2009.
 [4] Valcan, D.-M.; et al, "Connecting a PV supplied micro-grid to the public grid," in *Proc. of 11th International Conference on Optimization of Electrical and Electronic Equipment*, pp. 369-374, 22-24 May 2008.
 [5] Papanikolaou, N.P.; et al, "Analytical model for PV — Distributed generators, suitable for power systems studies," in *Proc. of 2009 European Conference on Power Electronics and Applications (EPE)*, pp.1-10, 8-10 Sept. 2009.
 [6] Bellini, A.; Bifaretti, S.; Iacovone, V., "MPPT algorithm for current balancing of partially shaded Photovoltaic modules," in *Proc. of 2010 IEEE International Symposium on Industrial Electronics (ISIE)*, pp. 933-938, 4-7 July 2010.
 [7] Li, R.T.H.; Chung, H.S., "Output current control for grid-connected VSI with LCL filter," in *Proc. of 2010 International Power Electronics Conference (IPEC)*, pp.1665-1670, 21-24 June 2010.
 [8] Rodriguez-Valdez, C.D.; Kerkman, R.J., "Phase Locked Loop for unbalanced utility conditions," in *Proc. of 2010 IEEE Applied Power Electronics Conference and Exposition (APEC)*, pp. 634-641, 21-25 Feb. 2010.
 [9] Luttamus, P.; Tuusa, H., "Model-based cascade control of three-level STATCOM with a tuned LCL-filter," *Proc. of 2011 IEEE Applied Power Electronics Conference and Exposition (APEC)*, pp. 1569-1575, 6-11 March 2011.
 [10] Mitsubishi Electric. Installations. *Product Documentation*. [Online] Jun 2007. http://www.mitsubishielectric.com/bu/solar/products/pdf/b7538_b.pdf
 [11] Erickson, M.J.; Lasseter, R.H., "Integration of battery energy storage element in a CERTS microgrid," in *Proc. of 2010 IEEE Energy Conversion Congress and Expo (ECCE)*, pp. 2570-2577, Sept. 2010.
 [12] Femia, N.; Petrone, G.; Spagnuolo, G.; Vitelli, M., "Optimization of perturb and observe maximum power point tracking method," *IEEE Trans. on Power Electronics*, , vol. 20, no. 4, pp. 963- 973, July 2005.

APPENDIX

TABLE I: CONVERTER COMPONENT VALUES

Component	Parameter Value
Converter rating	15kW, 480V
Filter input inductor ($L1$)	1.3mH
Filter output inductor ($L2$)	5.0mH
Filter capacitor ($C1$)	30 μ F
DC bus capacitor	1300 μ F

TABLE II: CONVERTER CONTROLLER GAINS

Gain	Parameter Value
Common P -vs.-freq	3.14 [rad/sec/(pu Power)]
uSrc K_p	3 [rad/sec/(pu Power)]
uSrc K_i	100 [rad/s ² /(pu Power)]
uSrc K_{pv}	200 [W/V]
uSrc K_{dv}	0.1 [W/(V/Sec)]
CurReg K_p	10 [V/A]
CurReg K_i	50 [V/(A Sec)]
CurReg K_{pv}	650 [W/V]
CurReg K_{dv}	0.034 [W/(V/Sec)]